Lawrence Berkeley National Laboratory

Title

Optimization of the size and shape of the scanning aperture in autocollimator-based deflectometric profilometers

Permalink

Journal

ISSN

Authors

Lacey, Ian
Geckler, Ralf D
Just, Andreas
et al.

Publication Date

DOI

Optimization of the size and shape of the scanning aperture in autocollimator-based deflectometric profilometers

Ian Lacey ⓘD, Ralf D. Geckler ⓘD, Andreas Just, Frank Siewert, Thomas Arnold, Hendrik Paetzelt, Brian V. Smith, and Valeriy V. Yashchuk

View Online   **Export Citation**   **CrossMark**

ARTICLES YOU MAY BE INTERESTED IN

Optimization of the size and shape of the scanning aperture in autocollimator-based deflectometric profilometers

Ian Lacey,[1,a] [ID] Ralf D. Geckler,[2] [ID] Andreas Just,[2] Frank Siewert,[3] Thomas Arnold,[4,5] Hendrik Paetzelt,[4]
Brian V. Smith,[6] and Valeriy V. Yashchuk[1]

AFFILIATIONS

[1] Advanced Light Source, Lawrence Berkeley National Laboratory, Berkeley, California 94720, USA

[2] Physikalisch-Technische Bundesanstalt, Bundesallee 100, D-38116 Braunschweig, Germany

[3] Helmholtz Zentrum Berlin für Materialien und Energie, Department of Optics and Beamlines, Albert-Einstein-Str. 15,
12489 Berlin, Germany

[4] Leibniz Institute of Surface Engineering (IOM), Permoserstr. 15, 04318 Leipzig, Germany

[5] Technische Universitaet Dresden, 01062 Dresden, Germany

[6] Engineering Division, Lawrence Berkeley National Laboratory, Berkeley, California 94720, USA

[a] Electronic mail: ilacey@lbl.gov.

ABSTRACT

Deflectometric profilometers based on industrial electronic autocollimators (ACs), as the ELCOMAT-3000, have become indispensable tools for precision form measurements of optical surfaces. A growing number of labs at synchrotron and free electron laser x-ray facilities are going for BESSY-II NOM-like versions of the AC-based profilometers. These tools have proven capable of characterizing state-of-the-art aspherical x-ray optics with an accuracy on the level of 100 nrad (root-mean-square) over the spatial frequency range limited by the size of the aperture used in the profilometer. Typically, a round aperture with a diameter of about 2.5 mm is used. Previous investigations have shown that with the optimally aligned 2.5-mm aperture, the spatial resolution of a NOM-like profilometer corresponding to the first zero-crossing of the optical transform function (OTF) is ~1.2 mm. In this paper, we investigate the performance of an AC ELCOMAT-3000 for a slope profilometer with different aperture sizes and shapes. The results of angular calibration of the AC equipped with circular and rectangular apertures placed at different distances from the AC are discussed. The calibration was performed at the Physikalisch-Technische Bundesanstalt using the original experimental arrangements, also discussed in the paper. The OTF measurements with the specially developed test sample with chirped surface slope profiles were performed at the Advanced Light Source X-Ray Optics Laboratory (XROL) in application to a new optical surface measuring system under development at the XROL. In the OTF measurements, we have shown that application of a rectangular aperture with dimensions of 1.5 mm × 3 mm improves the spatial resolution in the tangential direction by a factor of ~1.4 compared to that of the standard circular aperture of 2.5-mm diameter. We believe that the results of our investigations are crucial for reaching fundamental metrological limits in deflectometric profilometry utilizing state-of-the-art electronic autocollimators.

Published under license by AIP Publishing. https://doi.org/10.1063/1.5058710

I. INTRODUCTION

Deflectometric profilometers based on industrial electronic autocollimators (ACs) and a movable pentaprism have become indispensable tools for the precision form measurements of optical surfaces. This optical schematic was first suggested and realized at the Physikalisch-Technische Bundesanstalt (PTB) by Debler and Zander in 1978-1980 and by

Von Bieren in 1985.[1,2] The current, state-of-the-art version of such a profilometer, the so called Nanometer Optical Measuring Machine (NOM), was developed at the HZB/BESSY-II.[3,4] The profilometer is based on the ELCOMAT-3000 autocollimator made by Moeller Wedel Optical (MWO).[5] A large number of optical metrology labs at synchrotron and free electron laser x-ray facilities have AC-based profilometers in different arrangements.[6–12] These tools have proven capable of characterizing modern aspherical x-ray optics with an accuracy of the level of 100 nrad (root-mean-square, rms) over the spatial wavelength range limited by the size of the AC light beam aperture used and the maximum scanning length of the profilometer. In the case of shorter mirror lengths (<200 mm), mirrors with slope error better than 50 nrad (rms) have been measured.[4] Typically, in the AC-based slope profilometers, a circular aperture with a diameter of about 2.5 mm is used.[13,14] A smaller aperture size leads to an increase in the profilometer's systematic error and loss of stability (repeatability) of the measurements.

In this paper, we investigate the slope measurement performance of an ELCOMAT-3000 autocollimator equipped with circular and rectangular apertures with different sizes. The goal is to find an experimental arrangement providing higher lateral resolution of slope measurements with AC-based profilometers.

The increase in the resolution is especially important for slope metrology with highly curved aspherical x-ray mirrors fabricated using deterministic polishing technologies. In measurements with such optics, we have found that very often there is a periodic (quasi-periodic) residual slope error with the spatial period between ~2 mm and ~15 mm depending on the optic's shape, polishing process, mathematical algorithms applied to define the dwell time that determines the material removal rate in deterministic finishing technology,[15] and metrology tools and methods integrated into the fabrication process. With the current resolution of the AC-based slope profilometers of 1.2-1.6 mm, possible with a standard circular aperture, it is difficult (if not impossible) to satisfactorily characterize such high frequency periodic imperfections.

In the first part of the present paper, we discuss the results of angular calibration of an AC ELCOMAT-3000 recently purchased for the Advanced Light Source (ALS) X-ray Optics Laboratory (XROL).[16,17] We have tested a number of circular and rectangular apertures. We describe (Sec. II) an original design of the adjustable aperture systems used with a new Optical Surface Measuring System (OSMS)[18–20] under development at the XROL. The design of the aperture systems allows careful alignment of the aperture under test with respect to the AC optical axis as well as easy replacement of the apertures and readjustment of their size. The AC angular calibration was performed at the PTB using their sophisticated experimental method and setup[21–23] (Sec. III). In the course of the calibration (Sec. IV), we investigated the dependence of the AC systematic errors on the aperture size and shape as well as on the distances between the aperture and the AC. The major result of the performed angular calibration investigation is that the required high stability of AC measurements can be achieved with a rectangular aperture with the size of 1.5 mm (tangential) × 3 mm (sagittal).

Next, we discuss in detail the measurements of the AC spatial resolution or, more generally, its optical transfer function (OTF). For the OTF measurements, we use an original test sample with chirped surface slope profiles[24] developed by the collaboration of the HZB/BESSY-II and ALS metrology team and fabricated at the Leibniz Institut für Oberflächen Modifizierung (IOM) in Leipzig[25] (see Sec. V). The chirped profile sample is designed to have a constant (independent of spatial frequency) amplitude in the slope domain. In measurements with such a sample, we obtain highly confident information of the profilometer's resolution.[25] We provide (Sec. VI) a simplified analytical description of the one-dimensional (1-D) OTF of an AC equipped with circular and rectangular apertures. The spatial resolution measurements were carried out at the ALS XROL with the OSMS equipped with an ELCOMAT 3000 of the same model as the one calibrated at the PTB (Sec. VII). The AC was placed on the OSMS carriage in a downward facing orientation,[26] providing a constant distance to the sample surface while scanning the carriage with the AC along the chirped profile. This arrangement allows us to exclude the ambiguity of the calibration that can appear in the standard NOM-like arrangement utilizing a movable pentaprism that varies the AC-aperture distance during a measurement scan. Rectangular aperture with sizes preselected with the angular calibration was investigated (Sec. VIII). The results are compared to similar measurements with the standard 2.5-mm diameter circular aperture. The resolution investigation has demonstrated a significant improvement of the lateral resolution of the surface slope measurements with an AC equipped with a rectangular aperture with 1.5 mm width. On the basis of the performed investigation, we can conclude (Sec. IX) that usage of rectangular apertures in the AC-based profilometers, as suggested and discussed in the present work, opens a new avenue for surface slope measurements with improved resolution and reliability.

II. APERTURE SYSTEMS WITH ADJUSTABLE DIMENSIONS

The major goal of the angular calibration experiments is to determine a range of shapes and sizes of the aperture dimensions acceptable for AC applications in high accuracy surface slope metrology. We also need to check the AC measurement performance with the apertures placed at different distances from the AC. The most important are larger distances that correspond to the AC optical beam path present in a NOM-like profilometer with a stationary AC and a movable pentaprism.[3,4,6–11] In this case, we should expect a higher level of spurious effect due to AC light diffraction on the aperture. The shorter distances are interesting for the applications in surface slope profilers with a movable AC.[12,18–20]

For the calibration experiments, we have designed adjustable aperture systems with distances between 330 mm and 83 mm between the AC and the aperture under test–Fig. 2.

FIG. 1. The long distance aperture assembly that mounts to the tube of an ELCO-MAT 3000 autocollimator, with length L = 330 mm, equipped with adjustable circular apertures made of iris diaphragms. Note that the length is readily changed by removing sections of the extension tubing.

The aperture systems in Fig. 1 are designed for a direct mounting to the AC optical tube. At the side where the aperture system is mounted to the AC optical tube, there is a large iris diaphragm used to collimate the AC beam when aligning the aperture mounted on the opposite side. For the precise alig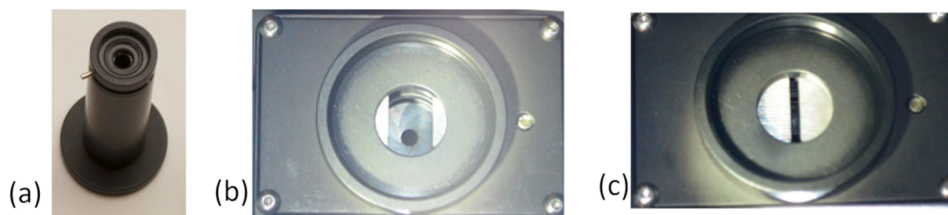nment of the apertures, we use the x-y kinematic stages and apply the method suggested and discussed in detail in Ref. 27. The closed design of the aperture systems was used to minimize air convection noise in the measurements.[20,28]

The design of the aperture systems allows easy replacement of different aperture assemblies (Fig. 2), each carrying one of three slit pieces with adjustable circular or rectangular apertures.

In the conventional NOM-like slope profilometer, a movable (preferably, mirror based[29,30]) pentaprism makes the measurement insensitive to the systematic error due to carriage wobble. But, the strong variation of the distance between the AC and the surface under test (SUT) in the course of mirror surface profile measurement makes it difficult to account for the AC systematic errors by application of an angular calibration performed at the fixed distance.[31]

Figure 3 shows the OSMS measurement arrangements with the long and short aperture assemblies mounted to the AC that is placed vertically on the OSMS translation carriage.[18–20]

In the course of the OSMS measurements when the carriage with the AC is translated along the SUT, the distance between the AC and the SUT is essentially unchanged.

FIG. 2. Replaceable aperture pieces that fit on the end of the extension tube (shown in Fig. 1) with adjustable circular apertures (a), and the one-dimensional slit opened to show the 3 mm circular aperture stacked above (b) and closed as used for the 1.5 mm × 3 mm rectangular aperture for high resolution tests (c).
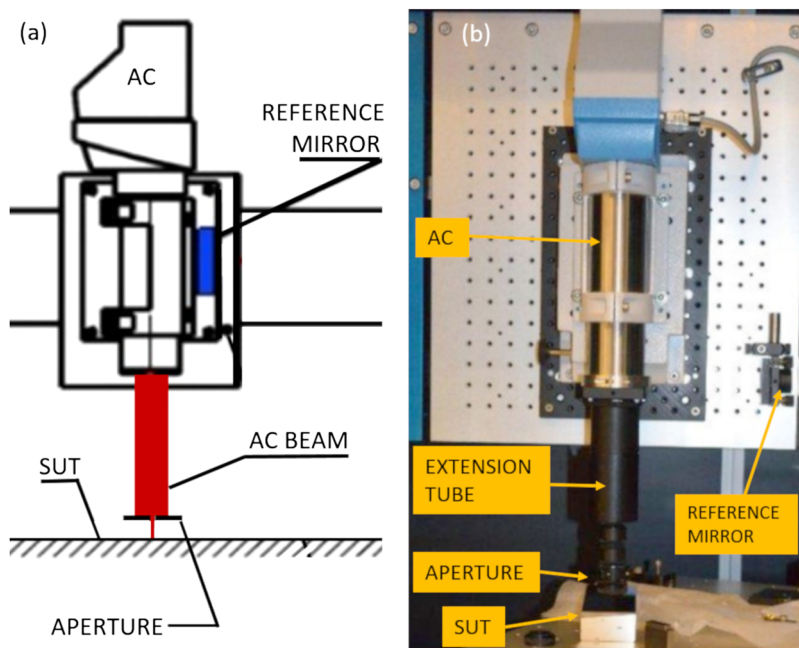

FIG. 3. The original schematic of the scanning gantry with a fixed distance autocollimator (a) and as implemented on the ALS OSMS (b), with the long distance aperture assembly attached to the AC.[18–20] Note that without a pentaprism to compensate for gantry wobble, a reference AC monitoring the reference mirror is needed to track the wobble of the scanning AC.

This allows application of the AC calibration performed at a dedicated facility (in our case, at the PTB; see Secs. III and IV, below) at the same AC-to-SUT distance for correction of the AC's systematic angle measuring errors. The payment for this advantage is a necessity to characterize and correct the wobbling error with an additional AC. To the best of our knowledge, the arrangement of an AC-based surface slope profilometer with a movable, vertically oriented AC and an additional AC in the reference channel was first considered in Ref. 26 and implemented and published in Refs. 12, 18–20.

III. ANGULAR CALIBRATION METHOD AND SETUP

AC calibrations with different apertures were performed with the primary angle standard of PTB, the WMT 220 angle comparator[21] manufactured by Dr. Johannes Heidenhain GmbH. The calibration is based on the comparison of the angle response of the AC to the comparator by use of a reference flat mirror mounted on its rotor. The angle comparator utilizes the subdivision of the full circle and circle closure, which obviates the need for any external angular reference for establishing an angular standard. The standard measurement uncertainty of the WMT 220 after calibration is about 5 nrad.[22,23] With a highly stable AC, calibration with standard uncertainty down to about 15 nrad is possible.[31–33] Following elaborate (and time consuming) shearing-based error-separation protocols, standard uncertainties down to 5 nrad have been achieved.[34]

Figure 4 presents the calibration setup at the PTB located in a clean room laboratory under highly stable environmental conditions (an ambient temperature variation of $\Delta T < 0.05$ K and a constant laminar air flow of $v = 20$ cm/s). The AC under calibration is mounted to a precision alignment stage, and the assembly is placed on a granite table at a desired distance from the aperture under test.
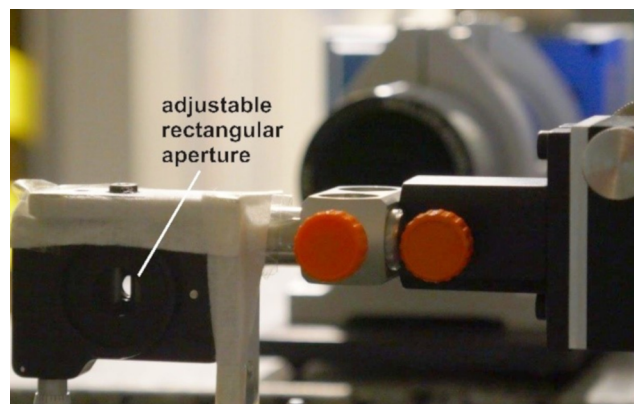

FIG. 5. The adjustable rectangular aperture assembly placed on the top of PTB's angle standard pictured from the direction of the reference mirror (with the mirror removed).

The aperture assembly and the reference mirror are mounted on the top of the rotor of the comparator. Figure 5 shows the aperture assembly placed in the front of the reference flat for AC calibrations. The assembly consists of a stacked iris diaphragm (which is used for the alignment of the assembly relative to the AC and restricts the beam footprint) and a slit of adjustable width (which restricts the beam in the horizontal direction).

Unfortunately, due to technical reasons, we could not apply the method for the precise centering of the apertures relative to the AC's optical axis described in Ref. 27. Instead, we used the laser attachment D65 by Möller-Wedel Optical (MWO)[35] for the adjustment of both the rectangular and circular apertures. For this purpose, the laser attachment was mounted temporarily to the AC tube so that the laser beam of the attachment marked the center of the tube carrying the
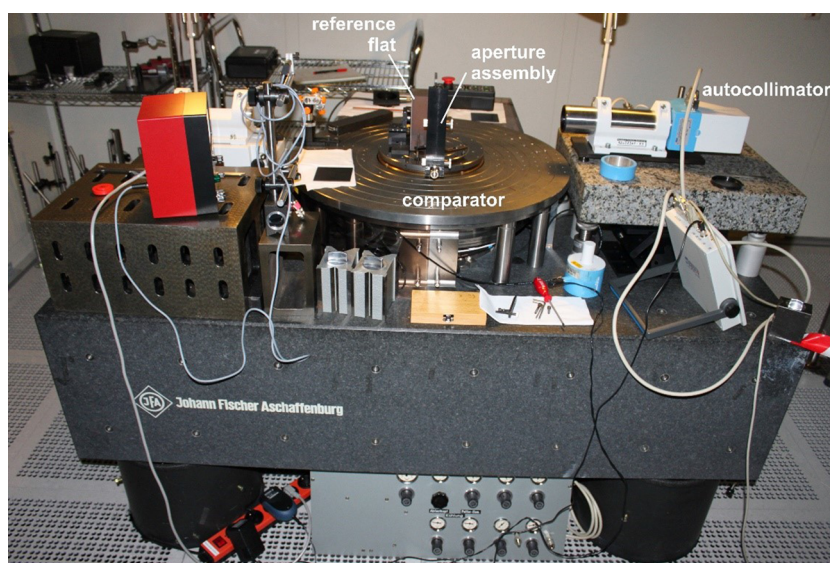

FIG. 4. The AC calibration setup based on the WMT 220 primary angle standard of PTB. Note that with the aperture assemblies placed on the rotation stage of the comparator, the apertures themselves rotate, whereas in use for the scanning gantry.

AC's objective (and, in good approximation, its optical axis). The iris diaphragm was opened to a diameter of approximately 2 mm and centered relative to the laser beam of the attachment.

In case of the calibration data sets with a rectangular aperture, the iris diaphragm was opened fully and the AC light beam was limited in the horizontal direction by the width of the slit. In case of the calibration data sets with a circular aperture, the aperture assembly was reverted and the slit was opened fully so that the beam footprint was restricted by the circular aperture only. The sizes of the apertures (the slit width and iris diameter) were adjusted by use of precision dowel pins. In both cases, the distance between the aperture closest to the mirror surface and the surface was approximately 5 mm.

With the rectangular aperture, the rotation angle of the aperture around the optical axis of the AC is an additional degree of freedom of the adjustment when compared to the circular aperture. For this adjustment, the casing of the AC was used as a mechanical reference.

Note that using the alignment procedure according to Ref. 27, one can refer to the reticle image cross-hash signal from the autocollimator for the axial alignment of the rectangular aperture. We have applied this method in the course of the resolution measurements with the OSMS (Sec. VII).

IV. RESULTS OF THE AC ANGULAR CALIBRATION

A. Dependence on the tangential width of rectangular apertures

First, we investigate the dependence of the AC calibration on the tangential width of the rectangular aperture. With the fixed sagittal width of 5 mm, we have performed a series of calibrations with three different tangential widths, 1.5 mm, 2 mm, and 3 mm. Figures 6 and 7 depict the results of the calibration over the angular ranges of ±97 μrad with steps of 0.48 μrad and ±4848 μrad with steps of 48 μrad, respectively.

Relatively large quasi-periodic systematic errors with two strong components with periods of approximately 6.4 μrad and 13 μrad are observed at 2 mm tangential width of the aperture, see Fig. 6, and—to a lesser extent—at widths of 1.5 mm and 3 mm, respectively. At the period of 13 μrad, the corresponding amplitude of the power spectral density (PSD) distribution obtained at 1.5 mm tangential width is smaller by a factor of ~2 compared to the aperture with 2 mm width.

The pixel width of the CCD detector of the ELCOMAT-3000 corresponds to an angular scale of 13 μrad. Errors with this period are caused by the interaction of the reticle image with the pixels of the CCD detector and the algorithms which determine the image shift on the detector by sub-pixel interpolation. Operating in the regime of aperture sizes below what the manufacturer recommends produces errors that increase with smaller apertures. Still, the shape of the error PSD distribution does not depend on the aperture's tangential width. The low-angular-period oscillations of the systematic error feature a period of ~315 μrad which is related to the reticle's
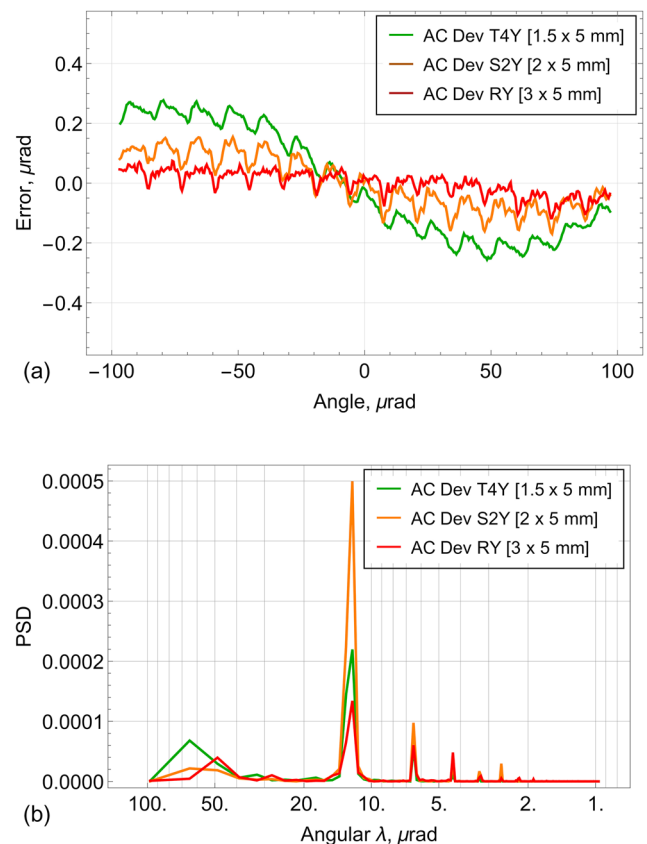

FIG. 6. (a) ELCOMAT-3000 autocollimator calibrations with rectangular aperture with the fixed sagittal width of 5 mm and three different tangential widths, 1.5 mm, 2 mm, and 3 mm. (b) The power spectral density distributions of the corresponding calibration traces given as the functions of the angular period. The calibrated tangential angular range is ±97 μrad.

geometry.[32] The 315-μrad-period error amplitude monotonically increases with the decrease in the tangential width of the rectangular aperture. However, the corresponding periods of the oscillations do not depend on the aperture size. Therefore, one still can use the correlation methods[19] for an effective suppression of the error.

The error at the lowest angular frequencies depicted in the PSD distributions in Fig. 7 with peaks with periods of about 1.6 mrad and 2.3 mrad is possibly due to the vendor calibration routine that removes a third order polynomial. As such, they do not depend on the size and shape of the apertures used in this work.

B. Selection of rectangular apertures to be used for the calibration

In the measurements as discussed in Sec. IV A, we have empirically found that decreasing the tangential width of a rectangular slit below approximately 1.2-1.3 mm leads to loss of the signal in the corresponding channel of the ELCOMAT-3000 autocollimator. With an aperture width of 1.5 mm and
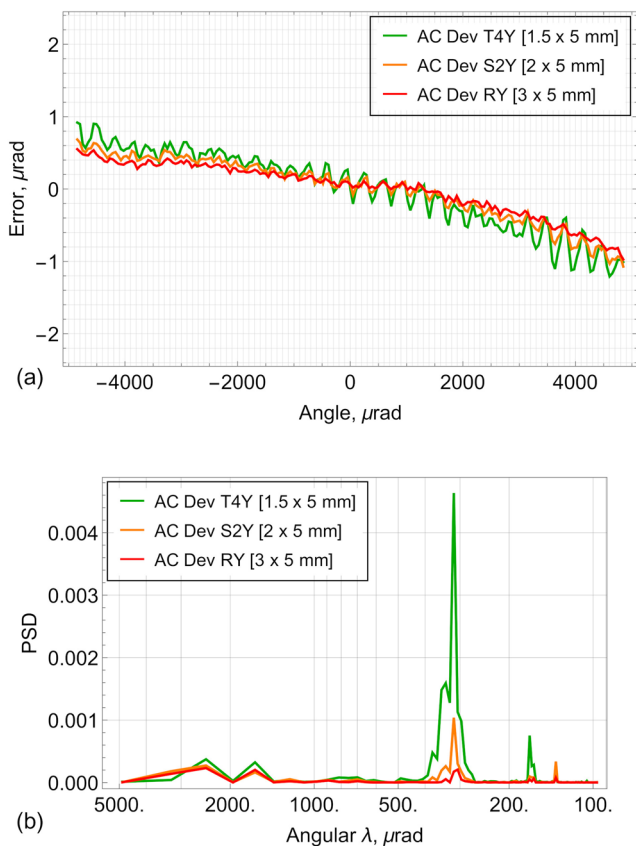
FIG. 7. (a) ELCOMAT-3000 autocollimator calibrations with rectangular aperture with the fixed sagittal width of 5 mm and three different tangential widths, 1.5 mm, 2 mm, and 3 mm. (b) The power spectral density distributions of the corresponding calibration traces given as the functions of the angular period. The calibrated tangential angular range is ±4848 μrad.
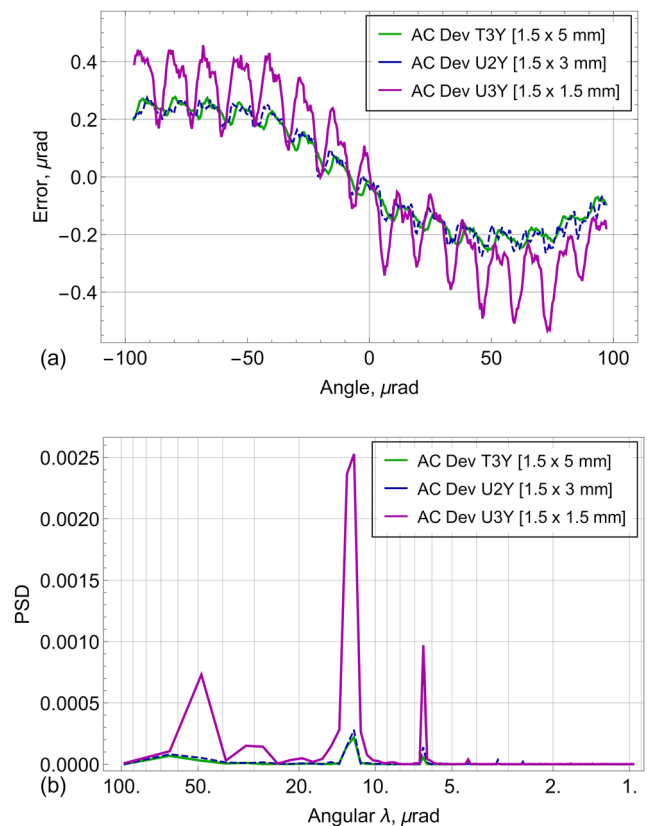

FIG. 8. (a) ELCOMAT-3000 autocollimator calibrations with rectangular aperture with a fixed tangential width of 1.5 mm and three different sagittal widths, 1.5 mm, 3 mm, and 5 mm. (b) The power spectral density distributions of the corresponding calibration traces given as the functions of the angular period. The calibrated tangential angular range is ±97 μrad.

larger, the AC provides stable measurements over the entire angular range of ±4.6 mrad.

In order to understand how the sagittal size of the aperture affects the measurements, we performed a series of calibrations with rectangular apertures with a fixed tangential width of 1.5 mm and three different sagittal widths, 1.5 mm, 3 mm, and 5 mm. The results are summarized in Figs. 8 and 9 depicting the calibration over two different angular ranges, ± 97 μrad and ±4848 μrad.

The measurements in Figs. 8 and 9 suggest that from the sagittal width of 3 mm–5 mm, the calibrations are practically not changed. Whereas, a significant difference is observed with the calibration at the sagittal width of 1.5 mm. Therefore, we have selected as optimal a rectangular aperture of 1.5 mm × 3 mm.

C. Comparison of calibrations with rectangular and circular apertures

The results of calibration of the same ELCOMAT-3000 autocollimator equipped with circular apertures of 2.5 mm

and 1.5 mm in diameter are presented in Figs. 10 and 11 for the calibration ranges of ±97 μrad and ±4848 μrad, respectively.

The decrease in the circular aperture to 1.5 mm diameter leads to a dramatic change in the amplitudes of the errors at all characteristic periods. The errors are significantly larger than those measured with the rectangular slit of 1.5 mm × 3.0 mm. Additionally, the stability (repeatability) of the calibration deteriorates. These results indicate that, for increasing the tangential resolution of slope measurements, it is advantageous to use a rectangular aperture with a decreased tangential width rather than a circular aperture of a smaller diameter.

V. TEST SAMPLE WITH CHIRPED PROFILE

For the spatial resolution measurement with the OSMS profilometer equipped with different apertures, we use an original test sample with two chirped surface slope patterns[24,25]−Fig. 12.

The two chirped surface slope patterns on the substrate have overlapping spatial frequencies. The lower frequency
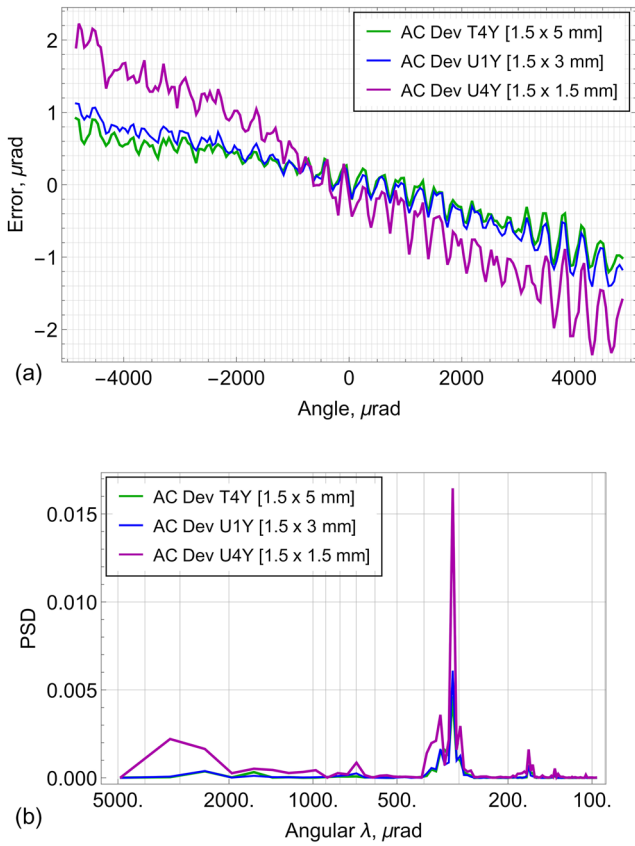
FIG. 9. (a) ELCOMAT-3000 autocollimator calibrations with rectangular aperture with a fixed tangential width of 1.5 mm and three different sagittal widths, 1.5 mm, 3 mm, and 5 mm. (b) The power spectral density distributions of the corresponding calibration traces given as the functions of the angular period. The calibrated tangential angular range is ±4848 μrad.
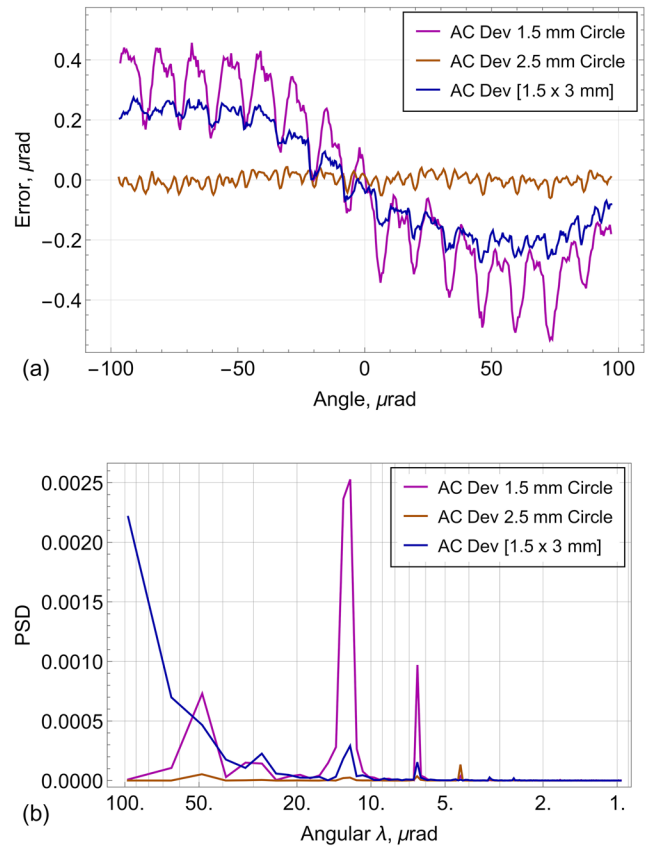

FIG. 10. (a) ELCOMAT-3000 autocollimator calibrations with two circular apertures of 2.5 mm and 1.5 mm diameter and 1.5 mm × 3 mm rectangular aperture. (b) The power spectral density distributions of the corresponding calibration traces given as the functions of the angular period. The calibrated tangential angular range is ±97 μrad.

pattern covers the spatial wavelength range from ~2 mm to ~7 mm, whereas the high frequency pattern covers the range from ~1 mm to ~4 mm. The chirped profiles are specified with the height distribution

$$h(x) = \frac{A_0}{2\sqrt{\omega_1}} \cdot S\left[2\sqrt{\omega_1} \cdot (x + x_0)^2\right], \quad (1)$$

where $S[z]$ is the Fresnel integral $\int_0^z \sin(\pi t^2/2)dt$. The profiles are designed to have a constant (independent on spatial frequency) amplitude and linearly increasing frequency in the slope domain described with

$$\alpha(x) = A_0 \cdot \sin\left[2\pi\omega_1 \cdot (x + x_0)^2\right]. \quad (2)$$

The PSD distribution of the slope profile in (2) is

$$PSD = A_0^2\left(1 - \sin\left[f^2/(4\pi\omega_1)\right]\right)(8\pi\omega_1)^{-1} \quad (3)$$

that describes the PSD oscillating with a constant amplitude and linear increasing frequency.

The values of the parameters in Eqs. (1)–(3) for the more dense chirped profile in Fig. 14 are $A_0 = 100\mu$rad,

$\omega_1 = 0.004$ mm^{-2}, and $x_0 = 25$mm and the interval of lateral positions of $x \in [0, 90]$ mm.

Figures 13 and 14 show the height profiles of the two chirped patterns, measured with a Fizeau interferometer, and their slope traces obtained by numerical differentiation of the corresponding height profiles. For an indication of the high quality of the chirped profiles, the lower frequency pattern was measured to have almost constant oscillation amplitude in the slope domain. There is a decrease in the oscillation amplitude with the increase in the spatial frequency, clearly seen in the slope profile of the higher spatial frequency chirped pattern. It can be attributed (at least partially) to the resolution limit of the interferometric measurements.

VI. APERTURE SHAPE AND THE OTF OF AN AC-BASED SLOPE PROFILOMETER

In this section, we put together a basic description of the effect of the aperture to the surface slope measurements of the chirped test sample with an AC-based
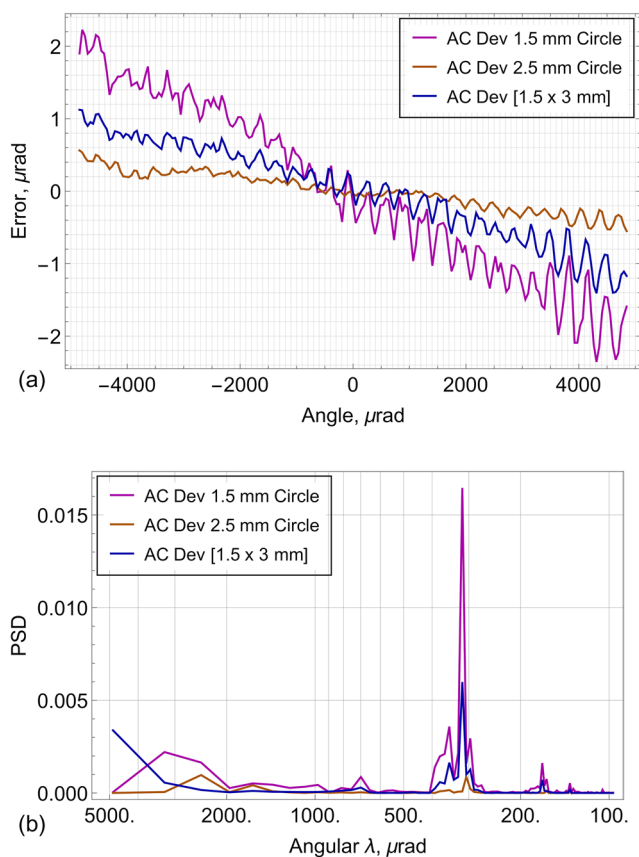
FIG. 11. (a) ELCOMAT-3000 autocollimator calibrations with two circular apertures of 2.5 mm and 1.5 mm diameter and 1.5 mm × 3 mm rectangular aperture. (b) The power spectral density distributions of the corresponding calibration traces given as the functions of the angular period. The calibrated tangential angular range is ±4848 μrad.
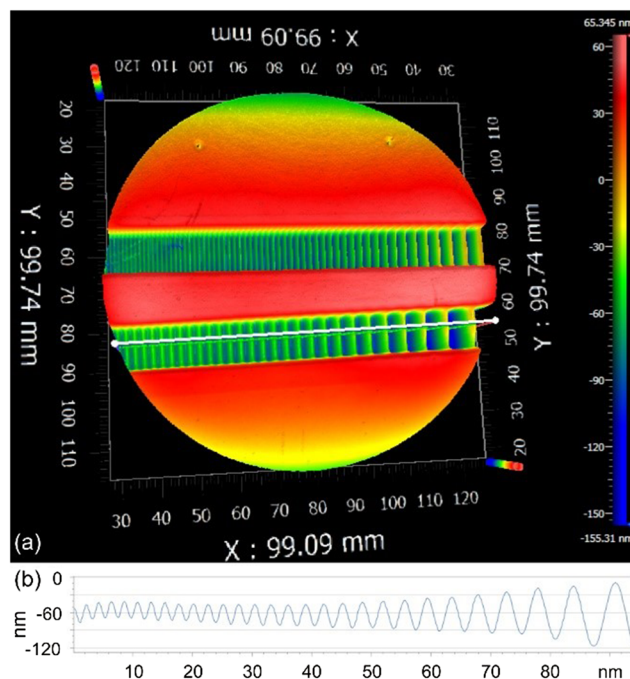

FIG. 12. (a) Test sample with two chirped surface slope patterns as measured with a Fizeau interferometer in the height domain. (b) Height profile of the slice shown in plot (a) with the white line. The profiles were fabricated on a 100 mm diameter silicon substrate by plasma jet etching.[25]
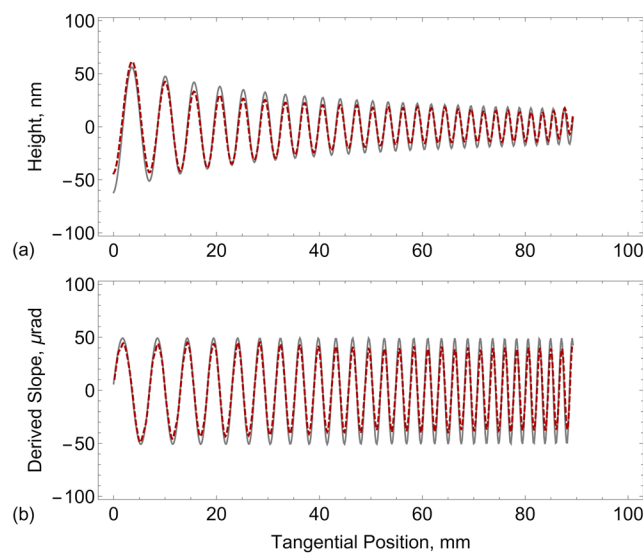

FIG. 13. (a) The measured height and (b) derived slope profiles of the lower spatial frequency chirped pattern of the used test sample obtained from measurements with a Fizeau interferometer in the height domain. The height and slope profiles measured with the sample are superimposed to the corresponding ideal (specified) distributions given with Eqs. (1) and (2) (the gray background lines).

surface profilometer. Here, we follow to the approach outlined in Ref. 36.

The aperture effect is characterized with the point spread function, PSF (see, for example, Refs. 28-39). In the case of an AC surface slope profilometer, the instrument's PSF has the physical meaning of the measured slope profile of a delta-function like surface slope perturbation (a step-function in the height domain). The effect of the PSF to the surface slope measurements can be thought of as application of the corresponding filter PSF to the topography under test. Mathematically, in the 1-D case, a measured trace α_{MES} is described as a convolution integral,

$$\alpha_{MES} = PSF * \alpha_{SUT} + N_{MES}, \qquad (4)$$

where α_{SUT} is the trace, corresponding to the inherent (unperturbed by the measurement) SUT topography. In Eq. (4), the symbol "*" denotes the convolution operation. The additive noise N_{MES} is due to random errors of the measurement. Here, we can ignore N_{MES} because the slope amplitudes of the
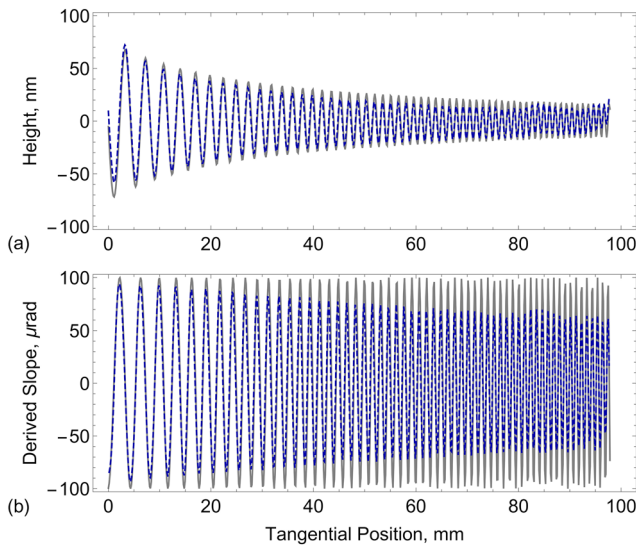
FIG. 14. (a) The measured height and (b) derived slope profile of the higher spatial frequency chirped pattern of the used test sample obtained from measurements with a Fizeau interferometer in the height domain. The height and slope profiles measured with the sample are superimposed to the corresponding ideal (specified) distributions given with Eqs. (1) and (2) (the gray background lines).

chirped sloped profiles are selected to be much larger than the measurement errors [see Figs. 13(b) and 14(b)].

The standard approach to analyzing the resolution property of a metrology tool is to present the resolution calibration measurements in the spatial frequency domain. When applied to (4), the Fourier transform of the PSF gives the OTF,[37]

$$Fourier[\alpha_{MES}] \equiv F[\alpha_{MES}] = F[PSF] \cdot F[\alpha_{SUT}] = OTF \cdot F[\alpha_{SUT}]. \quad (5)$$

The OTF closely relates to the instrumental modulation transfer function (MTF),

$$OTF \equiv MTF \exp(-iPTF). \quad (6)$$

The difference between the OTF and MTF is in the phase transfer function, PTF; see Eq. (6). For a symmetrical PSF centered on the ideal image point (this is usually the case of surface topology measurements with state-of-the-art profilometers), the PTF as a function of spatial frequency has only a value of either zero or π. Correspondingly, the OTF is a real bipolar function (with regions of positive and negative values), whereas the MTF is only positively defined.[37]

The phase dependence in the OTF is taken away by transforming Eq. (5) to the power spectral density domain,

$$PSD[\alpha_{MES}] = MTF^2 \cdot PSD[\alpha_{SUT}]. \quad (7)$$

In the case of the ideal chirped slope profile described with the constant-amplitude oscillating PSD given by Eq. (3), the squared instrument's MTF, MTF^2, has to be seen as an envelope over the oscillating measured PSD.

The oscillating PSD that is described in Eq. (7) is valid only in the case of infinitively long chirped sample. For measurements of a real chirped substrate of limited lateral size, the ideal PSD of the sample will be perturbed by the gate-function-like product to the infinitive chirped profile. The result of the simulations with the limited ideal chirped profile is presented in Fig. 15. In Fig. 15(a), the ideal (desired) limited chirped slope profile is shown. The corresponding PSD, calculated without adding any windowing, is depicted in Fig. 15(b). Because of the gate-function product effect, we can see the diffraction-like oscillations on the edges of the basically horizontal PSD in the spatial frequency range corresponding to the ideal chirped profile, Fig. 15(a). This PSD spectrum is used for comparison to measured results presented in Sec. VIII.

Next, we provide analytical models for OTF of the AC-based slope profilometers equipped with the optimal 1.5 mm × 3.0 mm rectangular aperture and the standard 2.5-mm diameter circular aperture.

A. Rectangular apertures

In the case of a 2-D rectangular aperture, the instrumental 2-D OTF is a product of two sinc-functions corresponding to the tangential and sagittal directions (see, for example, Refs. 38 and 39). In order to get the 1-D OTF describing the profilometer's resolution in the tangential direction, we integrate the sagittal sinc-function and obtain

$$OTF_u = \frac{\sin(\pi bu)}{\pi bu}, \quad (8)$$

where b is the tangential size of the aperture and u is the spatial frequency variable, corresponding to the tangential coordinate x. The 1-D OTF given with Eq. (2) with the tangential size $b = 1.5$ mm is depicted in Fig. 16 with the blue line.

B. Circular apertures

In the cases of a profilometer equipped with a circular aperture, the 1-D OTF is
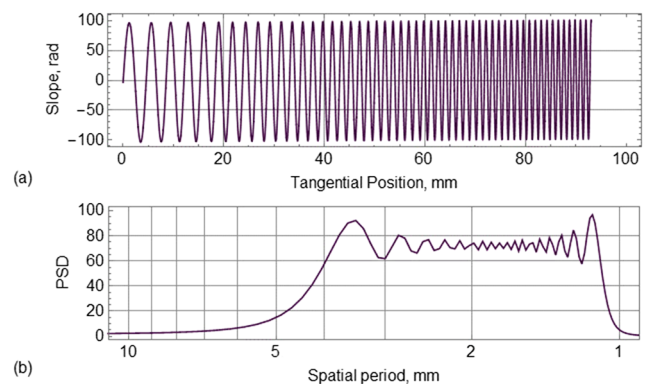

FIG. 15. (a) The ideal (desired) limited chirped slope profile and (b) the corresponding PSD.
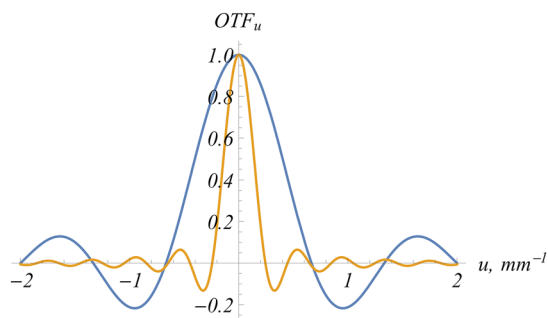
FIG. 16. Theoretical 1-D optical transform functions of an AC-based slope profilometer equipped with a rectangular aperture with the tangential size of 1.5 mm (the blue line) and a circular aperture with the radius parameter of 1.25 mm (the orange line).

$$\mathrm{OFT}_f = \frac{J_1(2\pi a u)}{\pi a u}, \tag{9}$$

where $J_1(2\pi a u)$ is the first order Bessel function of the first kind and a is the radius of the aperture. For an analytical expression for the corresponding 1-D point spread function, see, for example, Ref. 36.

The OTF, given with Eq. (9) and shown in Fig. 16 with the orange line, produces low-pass filtering effect with multiple zeros and negative regions where the contrast at those spatial frequencies is reversed. This effect was clearly observed in Refs. 24 and 25. The spatial wavelength, corresponding to the first zero-crossing, can be accepted as the measure of the instrumental resolution.

In Fig. 16, the larger overall width of the OTF of the 1.5×3.0 mm rectangular aperture is an indication of significantly higher spatial resolution compared to the circular aperture with a minimum possible diameter of 2.5 mm (see Sec. VIII).

Both OTFs in Fig. 16 are real bipolar functions with regions of positive and negative values. The corresponding squared MTFs are only positively defined with nonzero magnitude besides the points of zero crossing. If the slope profilometer's MTF is known (precisely measured) over the extended frequency range, it can be used for partial slope data restoration over the spatial frequency range above the resolution limit determined by the first zero-crossing of the OTF.[36]

The simple model used here predicts the first zero-crossings at the spatial wavelengths of 1.5 mm and 2.05 mm for the optimal tangential and the standard circular apertures, respectively. However, in publications[25] (see also the results of our measurements in Sec. VIII), it has been shown that with the optimally aligned 2.5-mm circular aperture,[27] the spatial resolution of a NOM-like profilometer is about 1.2 mm if the first zero-crossing of the OTF is assumed as a criterion for the spatial resolution achieved. Between the value measured in Ref. 25 and the prediction of the simple model (Fig. 16) is the resolution of the ALS DLTP[7,8] (equipped with an iris diaphragm adjusted to 2.5-mm diameter) estimated from autoregressive–moving-average (ARMA) modeling of data[40] measured with

the DLTP. The later result can be understood as a resolution in measurements with a high quality x-ray mirror that is limited by the measurement random error [compare with Eq. (4)].

VII. LATERAL CALIBRATION SETUP AND MEASUREMENT PROCEDURE

The spatial resolution measurements were carried out at the ALS XROL with the OSMS in the arrangement shown in Fig. 3(b). An AC ELCOMAT-3000 placed on the OSMS carriage in a downward facing orientation is of the same model as that used for the angular calibration at the PTB. The vertical orientation of the AC ensures a constant distance to the sample surface while scanning the carriage with the AC along the chirped profile. This allows us to exclude the ambiguity of the calibration that would appear in the standard NOM-like arrangement utilizing a movable pentaprism that varies the AC-aperture distance during a measurement scan.

The short (~83 mm) aperture system used for the spatial resolution measurements is shown in Fig. 17 as attached to the AC optical tube. For high accuracy alignment of the aperture under investigation with respect to the AC optical axis, we apply the procedure described in detail in Ref. 27. Using the procedure for the axial alignment of the rectangular aperture, we refer to the reticle image cross-hash signal from the autocollimator.

Exploiting the capability of the OSMS of 2-D scanning,[18-20] the forward and backward scanning of a single measurement run were arranged as depicted in Fig. 18. Thus, the measurements over the lower and higher frequency patterns and, additionally, along the unpatterned surface of the sample substrate were conducted in the course of a single, automated scan sequence, allowing us to avoid any uncertainty due to a possible temporal instability of the setup. For perspective, repeated measurements of the high frequency trace conducted a day apart had an 88 nrad (rms) repeatability with a drift equivalent to a curvature with a radius of 276 km.
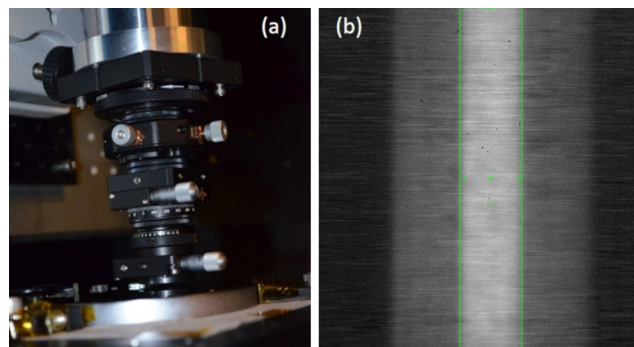

FIG. 17. Short aperture system used for the spatial resolution measurements with the ALS XROL OSMS (a), and the reticle image signal seen through the rectangular aperture, used for alignment (b).
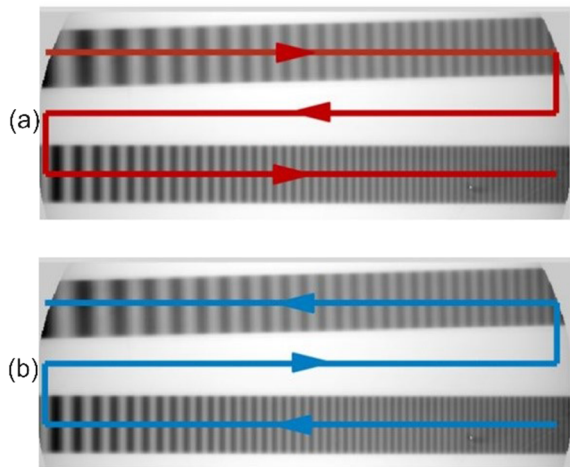
FIG. 18. Arrangement of the forward (a) and the backward (b) scans of a single OSMS run of measurement with the chirped test sample.

Four forward and backward scans, with a scanning gantry step increment of 0.1 mm, of a single run were arranged according to the optimal scanning strategy designed for suppression of drift errors described by the second order polynomial.[41]

VIII. RESULTS OF THE AC LATERAL CALIBRATION WITH DIFFERENT APERTURES

Figures 19 and 20 present the tangential slope distributions of the chirped sample measured with the OSMS AC equipped with the 2.5-mm circular and 1.5 mm × 3 mm rectangular apertures, respectively. The three traces shown in each figure correspond to the measurements conducted over the lower and higher frequency patterns [plots (a) and (c)] and along the unpatterned surface [plot (b)] of the sample substrate (compare with Fig. 18).

Significant improvement of the spatial resolution in the tangential direction results in a higher amplitude of the slope oscillations measured with the rectangular aperture over the both chirped patterns. While the AC with the circular aperture fails to measure the higher spatial frequency chirped pattern at the positions above ∼80 mm, the resolution of the AC equipped with the rectangular aperture allows reliable recording of the oscillations over the entire pattern.

Figure 21 shows the expanded detail of the plot (c) in Fig. 19 around the first zero-crossing at the position of ∼79 mm that corresponds to the spatial wavelength of ∼1.2 mm. Note that at the wavelengths shorter than 1.2 mm, the phase of the measured oscillation is reversed with respect to the slope oscillation inherent to the sample.

The improved resolution of the slope measurements with the rectangular aperture leads to the increased higher-spatial-frequency surface slope variation measured over the unpatterned traces [Figs. 19(b) and 20(b)]. Remarkably, the surface perturbation at the tangential position of about 15 mm
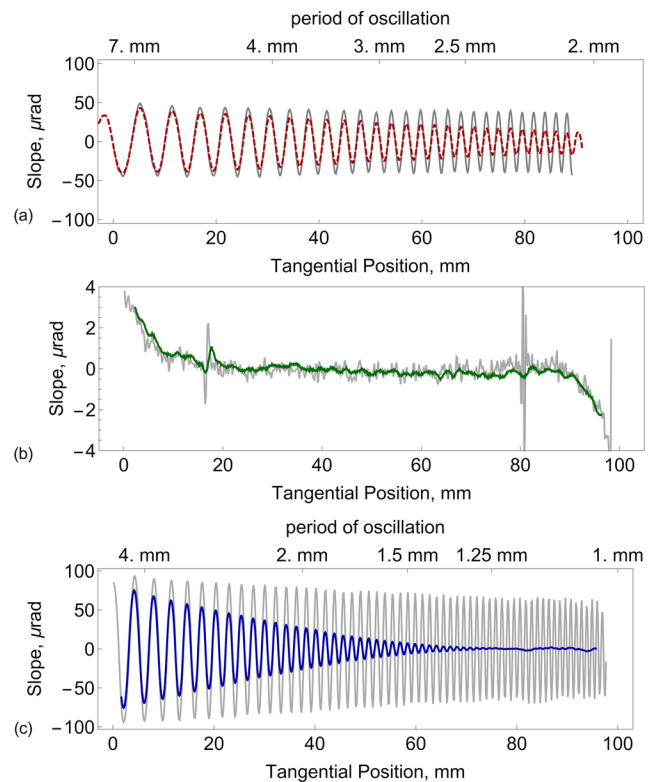

FIG. 19. The tangential slope distributions of the chirped sample measured with the 2.5-mm circular aperture over the lower and higher spatial frequency patterns [plots (a) and (c)] and along the unpatterned surface [plot (b)] of the sample substrate (compare with Fig. 18). The measured slope traces are superimposed to the corresponding sample slope distributions calculated from the interferometric measurements (the gray background lines).

has almost twice larger amplitude when measured with the rectangular aperture.

Using the frequency scale in Fig. 21, we can estimate the spatial resolution of the OSMS AC equipped with the 2.5-mm circular and 1.5 mm × 3 mm rectangular apertures to be about 1.2 mm and better than 1 mm, respectively.

The spatial frequency range of the chirped patterns of the present test sample is not enough for more precise measurement of the resolution of the AC equipped with the optimal rectangular aperture. We have designed and are working on the fabrication of a new test sample with an extended frequency range.

The PSD spectra of the slope distributions of the lower and higher spatial frequency chirped patterns measured with the OSMS AC equipped with the 2.5-mm circular and 1.5 mm × 3 mm rectangular apertures are shown in Figs. 22 and 23. The three PSD spectra shown in each figure correspond to the measurements conducted with the circular and rectangular apertures (bottom spectral lines and middle spectral lines) and to the calculation from the slope distributions
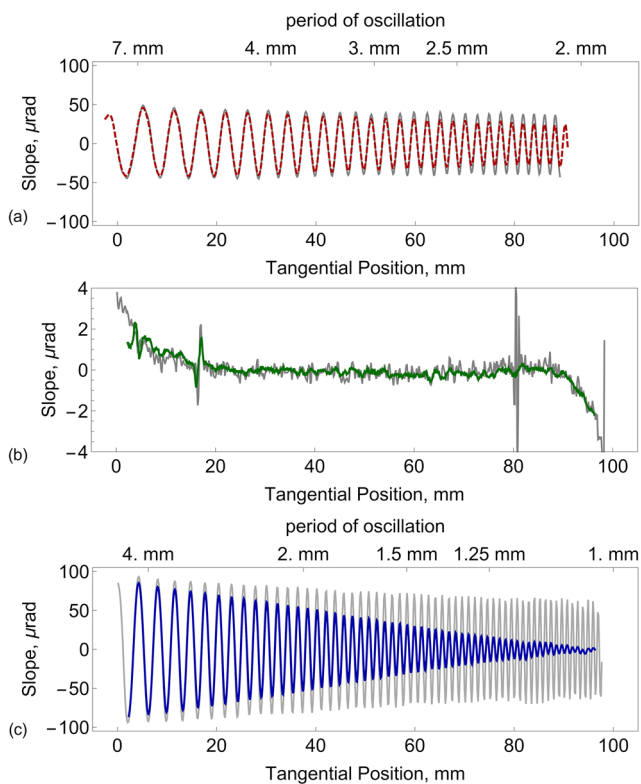
FIG. 20. The tangential slope distributions of the chirped sample measured with the 1.5 mm × 3 mm rectangular aperture over the lower and higher spatial frequency patterns [plots (a) and (c)] and along the unpatterned surface [plot (b)] of the sample substrate (compare with Fig. 18). The measured slope traces are superimposed to the corresponding sample slope distributions calculated from the interferometric measurements (the gray background lines).

evaluated from the interferometric height measurements with the corresponding pattern (top spectral lines) (compare with Fig. 15).
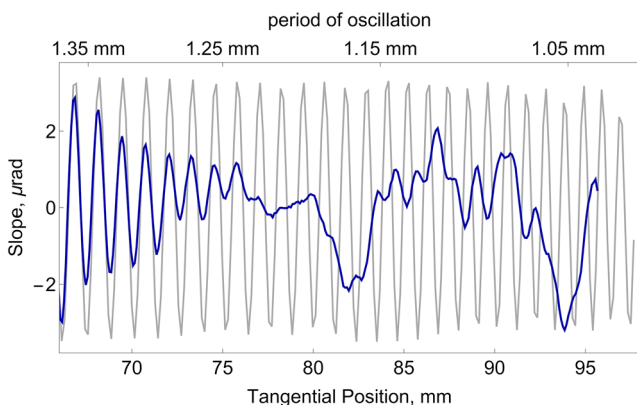

FIG. 21. Expanded detail of the plot (c) in Fig. 19 around the first zero-crossing at the position of ~79 mm that corresponds to the spatial wavelength of ~1.2 mm.
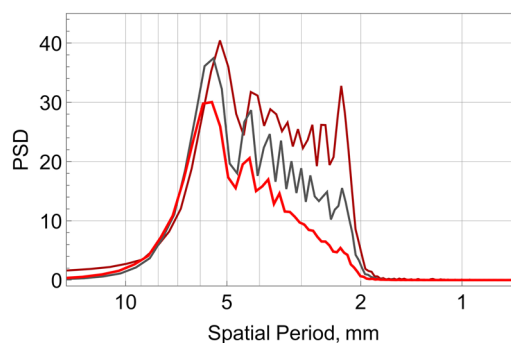

FIG. 22. PSD spectra of the slope distributions of the lower spatial frequency chirped pattern measured with the OSMS AC equipped with (bottom spectral line) the 2.5-mm circular aperture and (middle spectral line) 1.5 mm × 3 mm rectangular aperture. (top spectral line) PSD calculated from the slope distributions evaluated from the interferometric height measurements.

The PSD data in Figs. 22 and 23 confirm the major conclusion above that the spatial resolution in the tangential direction of the AC slope measurements is significantly improved by using the rectangular aperture. The PSD spectrum in Fig. 23(b), measured with the rectangular aperture, runs up to the highest spatial wavelength of ~1.1 mm, available with the sample. This is in contrast with the PSD spectrum measured with the circular aperture that is practically zeroed at the spatial wavelength of about 1.5 mm. Note that the simple OTF model depicted in Fig. 16 correctly predicts the degree of the resolution improvement.

Note that the sub-diameter effective spatial frequency cutoff of ~1.5 mm observed in the PSD spectrum measured with the standard circular diaphragm (Fig. 23) is in an excellent agreement with the results in Ref. 40 (see also discussion in Sec. VI B). However, this is slightly larger than the experimental results depicted in Fig. 21 and observed in Ref. 25, where the first zero-crossing of the measured slope oscillation appears at the wavelength of ~1.2 mm. Both resolution results
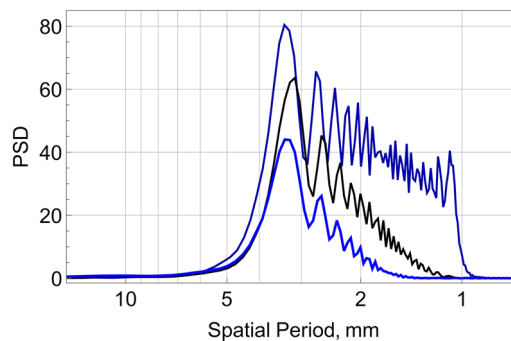

FIG. 23. PSD spectra of the slope distributions of the higher spatial frequency chirped pattern measured with the OSMS AC equipped with (bottom spectral line) the 2.5-mm circular aperture and (middle spectral line) 1.5 mm × 3 mm rectangular aperture. (top spectral line) PSD calculated from slope distributions evaluated from the interferometric height measurements.

significantly contradict (by a factor of about 1.5) the simple OTF model (Fig. 16) that predicts the first zero-crossings at the wavelengths of 2.05 mm and 1.5 mm for the circular and rectangular apertures, respectively. The discrepancy is probably because the simplified model does not account for the peculiarities of the data acquisition and processing of the autocollimator in use.

IX. CONCLUSIONS

In the present paper, we have first suggested and thoroughly investigated the usage of rectangular apertures with an electronic autocollimator in the arrangement of surface slope measuring profilometers. The performed investigations have shown that reliable surface slope measurements with the profilometer using an ELCOMAT-3000 autocollimator can be performed with a rectangular aperture with a tangential width as small as 1.5 mm and a sagittal width of 3 mm (and larger).

The tangential spatial resolution of the OSMS using an ELCOMAT-3000 autocollimator equipped with the selected 1.5 mm × 3 mm rectangular aperture has been characterized in the dedicated experiments with a test sample with two chirped surface slope patterns. We demonstrated that application of the rectangular aperture improves the spatial resolution by a factor of ~1.4 compared to the standard circular aperture with the diameter of 2.5 mm. This rectangular aperture shape, with 1.5 mm tangential width and 3 mm sagittal width, has much smaller quasi-periodic systematic errors than a square 1.5 mm aperture. These errors manifest themselves primarily as periodic signals with angular periods ~300 μrad (related to the reticle's geometry) and ~13 μrad (related to the interaction of the reticle image and the detector pixels). Note that improvement of the spatial resolution by decreasing the size of a circular aperture to 2 mm or less has been found to be unfeasible.

For the higher spatial frequency measurement, when we need to more reliably depict the amplitude of the higher spatial frequency periodic perturbations of the optical surface (e.g., due to the artifacts of the deterministic polishing processes—see e.g., Ref. 42), it is beneficial to select a smaller tangential aperture size. The higher spatial frequency information on the topography of optics allows more accurate simulation of the expected performance of beamlines.[43,44]

Usage of rectangular apertures in AC-based slope profilometers opens a unique opportunity for reliably combining measurements performed with low and high resolution (with large and small tangential widths of the aperture, respectively). In this case, the high-resolution measurements are detrended and filtered over the spatial frequency range depicted in the high accuracy measurement of the mirror's low spatial frequency figure. The resulting trace can be added to the low spatial frequency figure to get a high accuracy measurement over the entire frequency range accessible with the profilometer. Such combination of the slope trace data measured with circular apertures of different diameters is impossible because the data have different resolutions in the sagittal direction.

Based on the investigations discussed in the present paper, we have designed and purchased a set of fixed-shape rectangular apertures (including squares) that will be used with the ALS XROL OSMS and DLTP slope profilometers. The corresponding tests of the sagittal resolution with the different fixed-size apertures are in plan and will be discussed elsewhere.

In conclusion, the performed investigation provides a foundation for a deeper discussion of how to optimally arrange surface slope measurements with state-of-the-art x-ray optics applying different type of beam-shaping apertures and stitching procedures. This question closely relates to the problem of specification of x-ray mirrors in terms of surface slope errors in the tangential and sagittal directions that would provide adequate beamline performance estimations based on the corresponding measured residual slope variations.

We believe that the investigations we performed and discussed in this paper are crucial for reaching fundamental metrological limits in deflectometric profilometry utilizing state-of-the-art electronic autocollimators.

REFERENCES

[1] E. Debler and K. Zander, "Measurement of evenness on optical plane surfaces with autocollimator and pentagon prism," PTB-Mitt. **90**(5), 339–349 (1980).

[2] K. Von Bieren, "Pencil beam interferometer," U.S. patent 4,498,773 (12 February 1985).

[3] F. Siewert, T. Noll, T. Schlegel, T. Zeschke, and H. Lammert, AIP Conf. Proc. **705**, 847–850 (2004).

[4] F. Siewert, J. Buchheim, T. Zeschke, M. Störmer, G. Falkenberg, and R. Sankari, J. Synchrotron Radiat. **21**, 968–975 (2014).

[5] See https://www.haag-streit.com/moeller-wedel-optical/products/electronic-autocollimators/elcomat-series/elcomat-3000/ for ELCOMAT 3000, MÖLLER-WEDEL OPTICAL, GmbH.

[6] S. G. Alcock, K. J. S. Sawhney, S. Scott, U. Pedersen, R. Walton, F. Siewert, T. Zeschke, F. Senf, T. Noll, and H. Lammert, Nucl. Instrum. Methods Phys. Res., Sect. A **616**(2-3), 224–228 (2010).

[7] V. V. Yashchuk, S. Barber, E. E. Domning, J. L. Kirschman, G. Y. Morrison, B. V. Smith, F. Siewert, T. Zeschke, R. Geckeler, and A. Just, Nucl. Instr. and Meth. A **616**(2-3), 212–223 (2010).

[8] I. Lacey, N. A. Artemiev, E. E. Domning, W. R. McKinney, G. Y. Morrison, S. A. Morton, B. V. Smith, and V. V. Yashchuk, Proc. SPIE **9206**, 920603-1–920603-11 (2014).

[9] L. Assoufid, N. Brown, D. Crews, J. Sullivan, M. Erdmann, J. Qian, P. Jemian, V. V. Yashchuk, P. Z. Takacs, N. A. Artemiev, D. J. Merthe, W. R. McKinney, F. Siewert, and T. Zeschke, Nucl. Instrum. Methods Phys. Res., Sect. A **710**, 31 (2013).

[10] J. Nicolas and J. C. Martínez, Nucl. Instr. and Meth. A **710**, 24–30 (2013).

[11] S. Qian, R. D. Geckeler, A. Just, M. Idir, and X. Wu, Nucl. Instr. and Meth. A **785**, 206–212 (2015).

[12] S. Qian and M. Idir, Proc. SPIE **9687**, 96870D-1–96870D-10 (2016).

[13] R. D. Geckeler and A. Just, Proc. SPIE **6704**, 670407-1–670407-12 (2007).

[14] F. Siewert, J. Buchheim, and T. Zeschke, Nucl. Instrum. Methods Phys. Res., Sect. A **616**(2-3), 119 (2010).

[15] A. Seifert, AIP Conf. Proc. **879**, 459 (2007).

[16] V. V. Yashchuk, N. A. Artemiev, I. Lacey, W. R. McKinney, and H. A. Padmore, Proc. SPIE **9206**, 92060I-1–92060I-19 (2014).

[17] V. V. Yashchuk, N. A. Artemiev, I. Lacey, W. R. McKinney, and H. A. Padmore, Opt. Eng. **54**(10), 104104-1–104104-14 (2015).

[18] I. Lacey, J. Adam, G. Centers, G. S. Gevorkyan, S. M. Nikitin, B. V. Smith, and V. V. Yashchuk, Proc. SPIE **10385**, 103850D (2017).

[19] V. V. Yashchuk, G. Centers, G. S. Gevorkyan, I. Lacey, and B. V. Smith Proc. SPIE **10612**, 106120O-1–106120O-23 (2018).

[20] I. Lacey, K. Anderson, G. P. Centers, R. D. Geckeler, G. S. Gevorkyan, J. Grossiord, A. Just, T. Nicolot, B. V. Smith, and V. V. Yashchuk, Proc. SPIE **10760**, 1076002-1–1076002-20 (2018).

[21] R. Probst, R. Wittekopf, M. Krause, H. Dangschat, and A. Ernst, Meas. Sci. Technol. **9**, 1059–1066 (1998).

[22] A. Just, M. Krause, R. Probst, H. Bosse, H. Haunerdinger, C. Spaeth, and G. Metz, and W. Israel, Precis. Eng. **33**(4), 530–533 (2009).

[23] R. D. Geckeler, A. Link, M. Krause, and C. Elster, Meas. Sci. Technol. **25**, 055003-1–055003-10 (2014).

[24] F. Siewert, J. Buchheim, T. Höft, T. Zeschke, A. Schindler, and T. Arnold, Nucl. Instrum. Methods Phys. Res., Sect. A **710**, 42–47 (2013).

[25] F. Siewert, T. Zeschke, T. Arnold, H. Paetzold, and V. Yashchuk, Rev. Sci. Instrum. **87**(5), 051907-1–051907-8 (2016).

[26] V. V. Yashchuk, *Oral Presentation at the First Meeting on Development of a New Optical Surface Slope Measuring System−OSMS-I* (ALS, Berkeley, 2010).

[27] R. D. Geckeler, N. A. Artemiev, S. K. Barber, A. Just, I. Lacey, O. Kranz, B. V. Smith, and V. V. Yashchuk, Rev. Sci. Instrum. **87**(5), 051906-1–051906-8 (2016).

[28] V. V. Yashchuk, S. C. Irick, A. A. MacDowell, W. R. McKinney, and P. Z. Takacs, Proc. SPIE **6317**, 63170D-1–63170D-12 (2006).

[29] S. K. Barber, G. Y. Morrison, V. V. Yashchuk, M. V. Gubarev, R. D. Geckeler, J. Buchheim, F. Siewert, and T. Zeschke, Opt. Eng. **50**(5), 053601-1–053601-10 (2011).

[30] S. K. Barber, V. V. Yashchuk, R. D. Geckeler, M. V. Gubarev, J. Buchheim, F. Siewert, and T. Zeschke, Opt. Eng. **50**(7), 0073602-1–0073602-8 (2011).

[31] R. D. Geckeler and A. Just, Proc. SPIE **7077**, 70770B-1–70770B-12 (2008).

[32] R. Geckeler, A. Just, M. Krause, and V. V. Yashchuk, Nucl. Instr. and Meth. A **616**, 140–146 (2010).

[33] A. Just, M. Krause, R. Probst, and R. Wittekopf, Metrologia **40**, 288–294 (2003).

[34] R. D. Geckeler and A. Just, Meas. Sci. Technol. **25**, 105009 (2014).

[35] See https://www.haag-streit.com/moeller-wedel-optical/products/electronic-autocollimators/recommended-accessories for Attachment D40/D65, MÖLLER-WEDEL OPTICAL, GmbH.

[36] V. V. Yashchuk, G. Centers, Yu. N. Tyurin, and A. Yu. Tyurina, Proc. SPIE **9962**, 99620G-1–99620G-17 (2016).

[37] G. D. Boreman, *Modulation Transfer Function in Optical and Electro-Optical Systems* (SPIE Press, Bellingham, Washington, 2001).

[38] S. M. Kay, *Modern Spectral Estimation: Theory and Application* (Prentice-Hall, Englewood Cliffs, 1988).

[39] G. M. Jenkins and D. G. Watts, *Spectral Analysis and its Applications*, 5th ed. (Emerson-Adams Press, Boca Raton, 2007).

[40] Y. V. Yashchuk and V. V. Yashchuk, Opt. Eng. **51**(4), 046501 (2012).

[41] V. V. Yashchuk, Rev. Sci. Instrum. **80**, 115101-1–115101-10 (2009).

[42] F. Siewert, J. Buchheim, T. Zeschke, G. Brenner, S. Kapitzki, and K. Tiedtke, Nucl. Instrum. Methods Phys. Res., Sect. A **635** (2011) S52–S57.

[43] D. Schmitz, F. Siewert, and T. Zeschke, Nucl. Instrum. Methods Phys. Res., Sect. A **774**, 89–93 (2015).

[44] S. Roling, H. Zacharias, L. Samoylova, H. Sinn, T. Tschentscher, O. Chubar, A. Buzmakov, E. Schneidmiller, M. V. Yurkov, F. Siewert, S. Braun, and P. Gawlitza, Phys. Rev. Spec. Top.–Accel. Beams **17**, 110705 (2014).